Chemistry & Biology
Article

Structure-Guided Discovery of Phenyl-diketo Acids as Potent Inhibitors of *M. tuberculosis* Malate Synthase

Inna V. Krieger,[1] Joel S. Freundlich,[1,4] Vijay B. Gawandi,[1] Justin P. Roberts,[1] Vidyadhar B. Gawandi,[1] Qingan Sun,[1] Joshua L. Owen,[1] Maria T. Fraile,[3] Sofia I. Huss,[3] Jose-Luis Lavandera,[3,5] Thomas R. Ioerger,[2] and James C. Sacchettini[1,*]
[1]Department of Biochemistry and Biophysics
[2]Department of Computer Science and Engineering
Texas A&M University, College Station, TX 77843, USA
[3]Tres Cantos Medicines Development Campus, Diseases of the Developing World, GlaxoSmithKline, Madrid 28760, Spain
[4]Present address: Departments of Pharmacology and Physiology and Medicine, Center for Emerging and Reemerging Pathogens, New Jersey Medical School, University of Medicine and Dentistry of New Jersey, 185 South Orange Avenue, Newark, NJ 07103, USA
[5]Present address: Institute for Applied Molecular Medicine (IMMA), School of Medicine, Universidad CEU San Pablo, Campus Monteprincipe, Boadilla del Monte, 28668 Madrid, Spain
*Correspondence: sacchett@tamu.edu
http://dx.doi.org/10.1016/j.chembiol.2012.09.018

SUMMARY

The glyoxylate shunt plays an important role in fatty acid metabolism and has been shown to be critical to survival of several pathogens involved in chronic infections. For *Mycobacterium tuberculosis* (*Mtb*), a strain with a defective glyoxylate shunt was previously shown to be unable to establish infection in a mouse model. We report the development of phenyl-diketo acid (PDKA) inhibitors of malate synthase (GlcB), one of two glyoxylate shunt enzymes, using structure-based methods. PDKA inhibitors were active against *Mtb* grown on acetate, and overexpression of GlcB ameliorated this inhibition. Crystal structures of complexes of GlcB with PDKA inhibitors guided optimization of potency. A selected PDKA compound demonstrated efficacy in a mouse model of tuberculosis. The discovery of these PDKA derivatives provides chemical validation of GlcB as an attractive target for tuberculosis therapeutics.

INTRODUCTION

Despite the availability of good first- and second-line therapeutics to treat tuberculosis (TB), drug resistance, latency, and persistence render TB a continuing threat to public health and pose an urgent need for the development of novel drugs (World Health Organization, 2011).

The glyoxylate shunt, which plays a central role in fatty acid metabolism, has long been considered a potential vulnerability of *Mycobacterium tuberculosis* (*Mtb*) that could be exploited for developing antitubercular therapeutics (McKinney et al., 2000). The glyoxylate shunt is an anaplerotic bypass of the traditional tricarboxylic acid cycle that allows for incorporation of carbon from acetyl-coenzyme A (CoA) produced by fatty acid metabolism. This pathway is utilized in plants, fungi, and prokaryotes but is absent in mammals. *Mtb* has been shown to undergo significant metabolic alterations during the course of infection. This includes a shift from a reliance on carbohydrates to fatty acids as a principal source of carbon (Bloch and Segal, 1956). The increased reliance on fatty acid β-oxidation and gluconeogenesis in concert with a shift away from glycolysis during infection is supported by analysis of transcriptional profiles (Schnappinger et al., 2003; Talaat et al., 2004).

The glyoxylate shunt has been shown to play a crucial role in *Mtb* virulence, as isocitrate lyase, the first committed step of the pathway, is required for infection in activated macrophages and in animal models (McKinney et al., 2000). The shunt consists of two enzymes: isocitrate lyase (ICL), which hydrolyzes isocitrate into glyoxylate and succinate; and malate synthase (GlcB), which converts glyoxylate into malate using one molecule of acetyl-CoA. The shunt bypasses two CO_2-generating steps of the TCA cycle, allowing incorporation of carbon (via acetyl-CoA) and serves to replenish oxaloacetate under carbon-limiting conditions (Kornberg and Krebs, 1957). *icl1* is one of the most highly upregulated genes in *Mtb* under conditions that mimic infection (Timm et al., 2003). Further studies demonstrated the essentiality of the glyoxylate shunt for a persistent or chronic infection by showing that *Mtb* lacking *icl1* was unable to persist for longer then 3 weeks in a mouse (McKinney et al., 2000). Furthermore, a knockout of both isoforms of *icl* could not establish an infection in mice and was rapidly cleared (Muñoz-Elías and McKinney, 2005). A critical role of the glyoxylate shunt for virulence has been reported for other intracellular and fungal pathogens (Lorenz and Fink, 2001; Dunn et al., 2009).

Targeting ICL has been a challenge, largely due to its highly polar and small active site that becomes even more constricted during catalysis (Sharma et al., 2000). To date, the most widely used inhibitor of ICL in vitro is the succinate analog, 3-nitropropionate, which has an inhibitory constant (K_i) of 3 μM (Sharma et al., 2000). In contrast to ICL, GlcB has a much more "druggable" and large active site, consisting of a 20 Å × 7 Å cavity, which normally accommodates the pantothenate tail of the acetyl-CoA. The catalytic Mg^{2+} is located at the bottom of the cavity (Smith et al., 2003; Anstrom and Remington, 2006).

X-ray crystal structures of GlcB bound with substrate glyoxylate or products CoA and malate (Smith et al., 2003) show that the protein conformation is nearly identical regardless of the ligand (root-mean-square deviation [rmsd] < 0.5 Å), suggesting that catalysis occurs without significant structural rearrangements. In this article, we report our structure-based discovery of small molecule inhibitors of *Mtb* GlcB and pharmacological validation of GlcB as a drug target. One of the identified GlcB inhibitors with a reasonable potency and favorable toxicity, pharmacokinetic (PK) and pharmacodynamic (PD) profiles, has demonstrated efficacy in a mouse model of TB and could serve as the basis for a novel class of antituberculars.

RESULTS

Discovery of PDKA and Crystal Structure of GlcB-Inhibitor Complex

A focused library of 35 small molecules with a glyoxylate-like substructure were assayed against GlcB and ICL at a single concentration point of 40 μg/ml. Of these, 19 showed activity against GlcB. All of the GlcB active compounds were phenyl-diketo acids (PDKAs), exemplified by (*Z*)-2-hydroxy-4-oxo-4-phenylbut-2-enoic acid (Figure 1A). The parent PDKA exhibited an IC_{50} of 2.0 μM against GlcB and was inactive against ICL. Based on these initial findings, approximately 100 PDKA analogs were synthesized using readily available starting materials and straightforward chemical synthesis (Adams, 2008; Pais et al., 2002; Summa et al., 2004; Tumey et al., 2004; Zeng et al., 2008). A series of compounds was selected that demonstrated a good balance of enzyme inhibition and whole-cell activity. Aryl diketo acids have also been identified in drug discovery projects for other Mg^{2+}-dependent enzymes. These include HIV-1 integrase and hepatitis C virus-polymerase, where the keto acid moiety was found to coordinate the catalytic divalent metal cation (Egbertson, 2007).

These compounds had IC_{50}s against GlcB ranging from 20 nM to >100 μM. However, the minimal inhibitory concentrations (MICs) against cultured mycobacteria were, in certain cases, in disagreement with the enzyme inhibition level and had poor reproducibility. A time-dependent decrease of activity was observed in solutions of inhibitors left at room temperature, even during short periods of time. Using UV/visible spectroscopy (UV/Vis spectroscopy) and high-performance liquid chromatography (HPLC) analysis to assess the stability of our compounds, we found that the parent PDKA was stable in distilled, deionized water and organic solvents (dimethyl sulfoxide [DMSO], MeOH). However, it was unstable ($t_{1/2} \approx 3$ days) in cell growth media or any of several buffer solutions tested. The results from our HPLC-mass spectrometry (MS) analysis were consistent with retro-Claisen decomposition, with acetophenone as a product. We reasoned that the very high degree of conjugation encompassing the PDKA molecule was the driver of the retro-Claisen decomposition, in agreement with previous findings (Egbertson, 2007). To avoid this decomposition, we hypothesized that the addition of a group to the *ortho* position of the PDKA phenyl ring would twist the ring out of plane, reducing the degree of conjugation. The structure of the GlcB-PDKA complex showed a 37° degree twist of the phenyl ring of PDKA out of plane with the conjugated diketo moiety. Therefore, we predicted that the twist due to substitution should not significantly impact binding of *ortho*-substituted PDKAs to the enzyme. Substitution at the *ortho* position afforded an approximately 10-fold increase in compound stability to greater than 30 days and actually improved the IC_{50} (Table 1). Identical substitutions at the *meta* and *para* positions had no effect on stability. The extent of conjugation of the *ortho*-substituted phenyl diketo acids in solution was indeed reduced. This was evidenced by a blue shift of their respective UV absorbance peaks (λ_{max} values), when compared to PDKA and *meta*- and *para*-substituted compounds (Table 1). Moreover, the magnitude of this spectral shift correlates with stability.

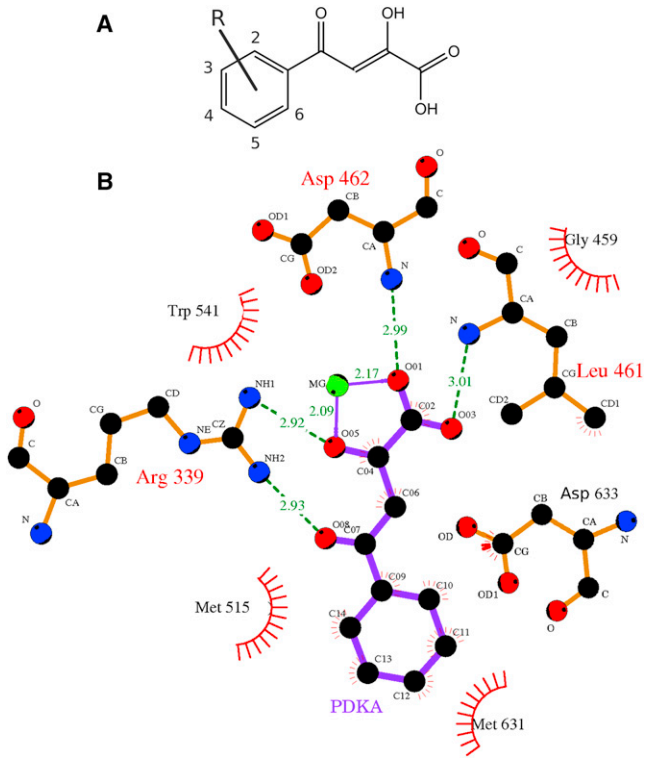

Figure 1. PDKA Inhibitor and Its Contacts to GlcB

(A) PDKA chemical structure drawn here in the enol form most consistent with solution-phase ^{1}H and ^{13}C nuclear magnetic resonance data.

(B) Diagram of PDKA-GlcB interactions; hydrogen bonds are shown in green. Catalytic Asp633 contacts the face of the phenyl ring. Coordinating interactions between the Mg^{2+} ion and oxygens of the inhibitor are in purple. Atom colors: black, carbon; red, oxygen; blue, nitrogen; green, magnesium. This figure was made in LigPlot (Laskowski and Swindells, 2011).

See also Figure S2.

All other attempts to stabilize this chemical framework (removing either of the two keto groups, replacing the carbon between them with a nitrogen, or introducing a methyl group to the β carbon of the diketo acid) resulted in compounds that were inactive against GlcB (data not shown). We evaluated replacements of the PDKA carboxylic acid by known Mg^{2+} chelators such as catechol and other bioisosteres such as tetrazole, but all of these failed to afford GlcB inhibitors with promising enzyme activity (IC_{50} > 100 μM).

In the crystal structure of the glyoxylate-bound *Mtb* GlcB, Cys619 was oxidized to cysteine-sulfenic acid, similar to *E. coli*

Table 1. Stability and Activity Data for PDKA Family Inhibitors

Compound	R	Half-Life (days)	λ_{max} (nM)	IC_{50} (μM)	MIC_{99} (μM) for *Mtb* mc^2 7000 Grown on Acetate	MIC_{99} (μM) for *Mtb* mc^2 7000 Grown on Dextrose
PDKA	Ph	3	340	2.0	50	25
1	2-MePh	30	326	1.1	>200	200
2	2-FPh	12	333	0.24	>200	200
3	2-ClPh	35	324	0.5	>200	200
4	2-BrPh	18	324	0.6	6.25	12.5
5	3-MePh	11	339	0.18	25	50
6	3-ClPh	7	341	0.17	25	25
7	3-BrPh	7	341	0.8	25	25
8	4-MePh	8	340	6.0	50	100
9	4-BrPh	7	345	5.7	50	25
10	2-Cl-6-FPh	>30	317	2.7	50	100
11	2-Cl-6-F-3MePh	>30	321	5.5	50	100

See also Table S1 and Figures S1 and S5.

malate synthase (Anstrom et al., 2003), resulting in a constriction at the entrance to the active site channel. The sulfenic acid is an artifact resulting from exposure to air during purification and is not relevant to the metabolic function of GlcB (Quartararo and Blanchard, 2011). We therefore constructed a Cys619Ala *Mtb* GlcB mutant, which exhibited ~80% of the reaction velocity of the wild-type (kinetic curve shown in Figure S1 available online). It also exhibited a 10-fold increase in acetyl-CoA K_M (from 5 to 50 μM). Examination of the crystal structure of GlcB bound to CoA (1N8W; Smith et al., 2003) shows that the Sγ of Cys619 forms a hydrogen bond with a nitrogen in the pantothenate arm of CoA. This could explain why the C619A mutant enzyme binds the cofactor with lower affinity, potentially causing the slight reduction in reaction velocity. A similar Cys619Ser *Mtb* GlcB mutant has also been described as a suitable model for kinetic studies (Quartararo and Blanchard, 2011). However, with the Cys619Ala mutant, we did not observe the lag in activity reported for the Cys619Ser mutant. Furthermore, elevating Mg^{2+} concentrations did not influence the activity (Figure S1). Since the IC_{50} values of inhibitors measured for the mutant and wild-type enzymes were well correlated (see Table S1; cf. Table 1), the C619A mutant protein was used in all subsequent crystallographic studies and enzyme assays. Cys619 is located ~5 Å away from the ligand (as shown in Figure S2) and thus does not participate significantly in binding of these inhibitors.

The crystal structure of GlcB (C619A) complexed with PDKA was determined at 1.9 Å resolution (data collection and refinement statistics are presented in Table 2). No significant conformational changes in the protein were observed upon PDKA binding compared to structures with glyoxylate or malate and CoA bound. The backbone rmsd of the superposition between the GlcB:malate complex and the GlcB:PDKA complex is 0.32 Å over 700 Cα atoms. Among 15 active site residues, the all-atom rmsd is 0.21 Å, excluding Met631, which adopts a different conformation to accommodate the phenyl ring. The diketo acid group of the PDKA coordinates the Mg^{2+} ion in an edge-on fashion, very similar to that of glyoxylate (Smith et al., 2003). The inhibitor fills two of the six octahedral coordination sites with one of the carboxylate oxygens and the adjacent ketone oxygen (2.1 Å and 2.2 Å contact distances, respectively). Other active site interactions are illustrated in Figure 1B. Carboxylate oxygens of the inhibitor hydrogen-bonded with the backbone nitrogens of Asp462 and Leu461 ($d_{O\text{-}N}$ = 3.0 and 3.0 Å, respectively). Both ketone oxygens also form hydrogen bonds ($d_{O\text{-}N}$ = 2.9 and 2.9 Å) with the Arg339 side chain, exhibiting similar contacts as the substrate and product. The catalytic Asp633 (Clark et al., 1988) side chain oxygen was within hydrogen-bonding distance (3.2 Å) to the phenyl ketone oxygen of PDKA. As noted earlier, the aryl ring of the PDKAs was twisted 37° out of coplanarity with the ketone. It occupied the approximate middle of the active site channel, overlapping the region where the thiol group of CoA normally binds. The aromatic ring forms multiple van der Waals interactions with the Cγ of catalytic Asp633 and the side chains of Met515, Trp541, and Met631. The carboxylate of the side chain of Asp633, which is expected to be deprotonated in view of its catalytic function (Clark et al., 1988), is positioned over the face of the PDKA ring. The carboxylate is slightly shifted toward the diketo acid side, with distances from Oδ1 to PDKA atoms C1 and C6 of 4.1 and 3.4 Å, respectively, and from Oδ2 to C1 and C2 of 3.3 and 4.0 Å, respectively.

The close contact between the Asp633 side chain and the aryl ring of the inhibitor is unusual. It resembles anion-π interactions that have recently been reported in small molecules and proteins (Berryman et al., 2007; Schottel et al., 2008). In most interactions between anions and aromatic groups in biomolecular systems, the anion contacts the aromatic ring on the edge (coplanar) with distances of ~4.5 Å. In contrast, the contacts of carboxylates over the center of the ring are generally >5.0 Å (Jackson et al., 2007; Philip et al., 2011). However, face-on anion-π contacts have been observed in inorganic systems and are enhanced by electron-withdrawing substituents, resulting in lower contact distances and higher binding affinities. This is supported by semiempirical quantum mechanics calculations for representative model systems that suggest there is a significant energy well for face-on contacts at 3–4 Å (Berryman et al., 2007; Schottel et al., 2008). All crystal structures of GlcB-inhibitor complexes with PDKA analogs we have solved to date exhibit

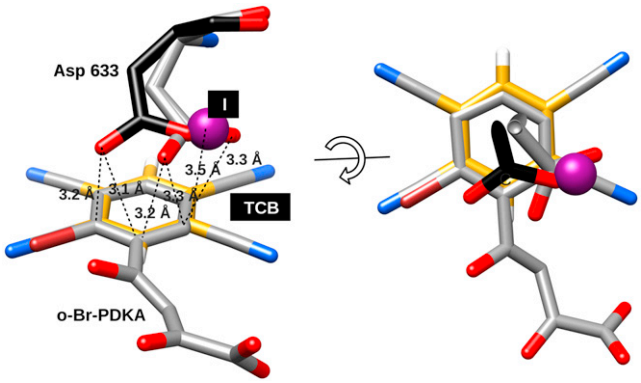

Figure 2. Anion-π Interaction

PDKA inhibitor (**4**) with Asp633 superimposed with crystal structure of TCB in complex with NaI (606750 entry at Cambridge Crystallographic Data Center as supplementary for small molecule anion-π complex structures; Berryman et al., 2007) colored by element, TCB ring is slightly offset for easier visualization. Halide shown as a purple sphere, TCB carbons are indicated as yellow; Asp633 with gray carbons represent Asp633 position in complex with single *ortho*-halogen-substituted PDKAs (o-Br-PDKA shown), while Asp633 with black carbons represent Asp633 position for all other complexes (with PDKA, **1**, **7**, and **11**). Atom colors: black, gray, or yellow, carbon; red, oxygen; blue, nitrogen; white, hydrogen; purple, iodine. Images are rendered in CHIMERA (Pettersen et al., 2004).

a close contact between the carboxylate of Asp633 and the face of the aromatic ring of the inhibitor. Among the five structures reported in this article, the mean distance between the closest arene carbon and either of the Asp633 oxygens is 3.1 Å, with a mean contact angle of 55° relative to the ring plane. This is consistent with a face-on interaction. A superposition of the ring plane of the Asp633-PDKA pair with the small-molecule crystal structure of tetracyanobenzene (TCB) complexed with iodide (NaI) reported by Berryman et al. (2007) (Figure 2) shows a very similar configuration between the two systems. The anion of the TCB-NaI complex (iodine) superimposes on the carboxylate of Asp633 in the GlcB-PDKA structures and is located over the periphery of the ring (the carbon connecting to the diketo acid moiety), rather than directly over the ring center as suggested by theoretical calculations (Schottel et al., 2008). Presumably, this position provides additional localized polarization. Anion positioning over the periphery of the ring rather than over the center has been hypothesized to indicate a partial charge-transfer character to the interaction (Berryman et al., 2007). In single *ortho*-halogen-substituted PDKAs (represented in Figure 2 by o-Br-PDKA) bound with GlcB, Asp633 is shifted away from the halogen by 1.7 Å (measured at Oδ2), reflecting the asymmetry created by the electron-withdrawing group. In contrast, with the symmetric double *ortho*-halogen-substituted PDKA, the carboxylate of Asp633 is in the same position as with unsubstituted PDKA or o-Me-PDKA (Figure 2).

Given the extra room in the active site around the phenyl ring of the PDKA, we hypothesized that an alternative cyclic structure could be accommodated and might improve affinity. Several replacements for the phenyl ring in PDKA were prepared, including aliphatic moieties, exemplified by cyclohexyl and adamantyl cores. But these were found to be inactive against GlcB (data not shown), suggesting a strong requirement for an aromatic moiety. Other aromatic rings such as naphthyl and various heterocycles were evaluated but were not immediately pursued due to a suboptimal combination of enzyme inhibition, whole-cell activity against cultured mycobacteria, and pharmacokinetic profile (full structure-activity relationship [SAR] data to be published elsewhere). Naphthyl-, indole-, pyrrole-, and thiophene-based diketo acids were active against the enzyme with IC_{50}s ranging from 20 nM to 5 μM. However, the first three did not exhibit adequate whole-cell activity, and thiophenes had only low whole-cell activity (≥50 μM) (attributed to albumin binding) (data not shown). Furan-, quinoline-, benzodioxole-, and benzothiazole-based PDKAs exhibited low enzyme inhibition activity (IC_{50}s ranging from 30 to 100 μM). Thiazole-, pyridine- and pyrimidine-based PDKAs were inactive against the enzyme (data not shown).

Structure-Guided Optimization of PDKA Analogs with High Potency

Structural examination of the GlcB-PDKA complex suggested several opportunities to enhance affinity by making substitutions around the PDKA aromatic ring to optimize interactions within the active site (a schematic view of substitution strategy is shown in Figure S3). Because of their importance for stability, we focused on optimizing the potency and whole-cell activity of *ortho*-substituted PDKAs. Crystal structures of complexes of GlcB with 20 of the synthesized PDKA analogs were determined at resolutions ranging from 1.8 to 2.2 Å to evaluate whether binding modes agreed with our predictions and to guide new ideas (crystallographic statistics for five representative data sets are shown in Table 2; an example of omit map density is shown in Figure S2). The crystal structure of GlcB in complex with 2-Br-PDKA (**4**) showed that the Br oriented toward the Val118 side chain (Figure 3A). The potency of the *ortho*-substituted analogs was improved compared to unsubstituted PDKA (2.0 μM). The most potent were those with halogens, with a preference for smaller groups: 2-F (0.24 μM) < 2-Cl (0.5 μM) < 2-Br (0.6 μM) < 2-Me (1.1 μM) (Table 1). This was presumably due to the increase of steric clashes with the Val118 side chain (3.2 Å from Br to the closest Cγ of Val118). There is little space available to accommodate a larger group. Indeed, o-Et-PDKA showed an IC_{50} of only 35 μM. Crystal structures of *ortho*-substituted PDKA complexes with GlcB indicated that all the *ortho* substituents orient in the same direction i.e., none are rotated to position 6 (Figure 1A), regardless of their size or nature. The ring of the *ortho*-substituted PDKA does not overlap exactly with the position of the parent PDKA ring (Figure 3). For all of 2-substituted inhibitors, it is moved about 0.7 Å away from Val118 to accommodate the group at the 2 position.

There was less room in the pocket off the 6 position of the aryl ring compared to the 2 position of the bound PDKA (3.9 Å to Leu461 compared to 4.4 Å to Val118). This is likely the reason why the double *ortho*-substituted compound 2-Cl-6-F (**10**) (IC_{50} = 2.7 μM) did not show better inhibition of the enzyme than PDKA (IC_{50} = 2.0 μM). However, we cannot rule out the possibility of an unfavorable alteration in the ring's charge distribution compared to a single *ortho*-substituent affecting interaction with Asp633 (Figures 3A and 3B).

Table 2. Crystal Data Collection and Refinement Statistics

Statistic	GlcB Complex with PDKA	GlcB Complex with **4**	GlcB Complex with **1**	GlcB Complex with **7**	GlcB Complex with **11**
Data Collection					
Space group	$P4_32_12$	$P4_32_12$	$P4_32_12$	$P4_32_12$	$P4_32_12$
Cell Dimensions					
a, *b*, *c* (Å)	79.33, 79.33, 225.94	79.45, 79.45, 226.26	77.74, 77.74, 221.98	78.22, 78.22, 223.58	78.49, 78.49, 224.05
α, β, γ (°)	90, 90, 90	90, 90, 90	90, 90, 90	90, 90, 90	90, 90, 90
Resolution (Å)	50–1.90 (1.93–1.9)	43.05–1.80 (1.83–1.80)	44.13–1.82 (1.92–1.82)	49.57–2.04 (2.13–2.04)	45.59–2.20 (2.24–2.20)
R_{sym} or R_{merge}	0.109 (0.532)	0.191 (0.634)	0.108 (0.554)	0.099 (0.584)	0.183 (0.742)
$I/\sigma I$	13.8	14.0	6.4	6.3	9.0
Completeness (%)	99.9 (99.4)	97.2 (76.0)	99.9 (100)	99.2 (98.6)	99.9 (100)
Redundancy	13.1 (10.2)	9.5 (2.6)	9.7 (9.8)	15.3 (15.4)	14.4 (14.8)
Refinement					
Resolution (Å)	50–1.90	43.05–1.8	44.13–1.82	49.57–2.04	45.59–2.2
No. of reflections	57789	66563	62029	45023	36507
R_{work}/ R_{free}	0.168/0.203	0.175/0.219	0.170/0.220	0.163/0.204	0.172/0.223
No. of atoms					
Protein	5,543	5,645	5,562	5,509	5,429
Ligand/ion	14/3	15/3	15/3	15/3	17/3
Water	674	859	641	574	400
B factors					
Protein	27.86	29.64	21.22	32.13	34.69
Ligand/ion	30.47/28.14	20.7/32.13	14.24/27.53	30.1/38.4	28.87/39.3
Water	39.65	40.55	28.79	38.58	40.78
Rmsd					
Bond lengths (Å)	0.013	0.007	0.007	0.007	0.008
Bond angles (°)	1.03	1.024	1.013	1.013	1.062

Data restricted to highest resolution shell are shown in parentheses. All crystals were of the C619A mutant enzyme with His_6 tag.
See also Figure S2.

Position 4 (*para*- to the diketo acid) points directly at the Met631 side-chain (3.6 Å to Met631 Cγ) (Figures 3A and 3B). Therefore, accommodation of a substituent at this position requires the Met631 side chain to assume a different conformation. Indeed, 4-Me and 4-Br PDKA analogs (**8** and **9**) showed higher IC_{50} values than parent PDKA (5.7 and 6.0 μM, respectively), likely due to steric interference with the Met631 side chain.

The structure of the PDKA bound to GlcB showed that position 3 of the aromatic ring was the most promising for extending the PDKA. Any extension should align with the long axis of the channel where the substrate acetyl-CoA binds (Figure 3). This offered the possibility of exploiting the pantothenate binding contacts. These include a hydrogen bond with the backbone N of Val119, and van der Waals interactions with the side chains of Met631, Met515, and the backbone of Val118-Val119. Indeed, analogs with substitutions at the *meta* position showed the largest improvement in potency over PDKA. The most active compounds were 3-Cl-PDKA (**6**, IC_{50} = 0.17 μM) and 3-Me-PDKA (**5**, IC_{50} = 0.18 μM). The crystal structure of GlcB in complex with the 3-Br-PDKA (IC_{50} = 0.8 μM) (**7**) showed the Br making van der Waals contacts, sandwiched between the side chains of Met515 and Met631, arranged on opposite sides of the channel. It is interesting to note that, although sufficient space seemed to exist in the channel to accommodate longer substitutions at the *meta* position, alkyl and $(CH_2)_nAr$ (n = 1, 2; Ar = aryl) substitutions at that position resulted in inhibitors with poor enzyme activity (IC_{50} > 100 μM). This may be attributed to a suboptimal angle at which the *meta* substituents project off the phenyl ring. This could potentially result in steric clashes with either Met631 or with Val119 and Pro120 on the other side of the channel.

The substituent's effect on the electronic properties of the aromatic ring of PDKA appeared to be critical for inhibition activity. This is likely due to their influence on ring π-interactions with the carboxylate of catalytic Asp633. For example, 2-Cl-6-F substituted PDKA (**10**) has an IC_{50} of 2.7 μM. In contrast, 2,6-Me-PDKA, which is of similar size and substitution positioning but not as electron withdrawing, was inactive, with an IC_{50} > 100 μM. Although the activity of compounds with halogens substituted at the 3 position had better enzyme activity than analogs substituted at the 2 position (e.g., 0.5 μM IC_{50} for 2-Cl-PDKA versus 0.17 μM for 3-Cl-PDKA), there was a tradeoff with stability. Two-substituted compounds exhibited longer half-lives. Since stability was important for whole-cell assays and

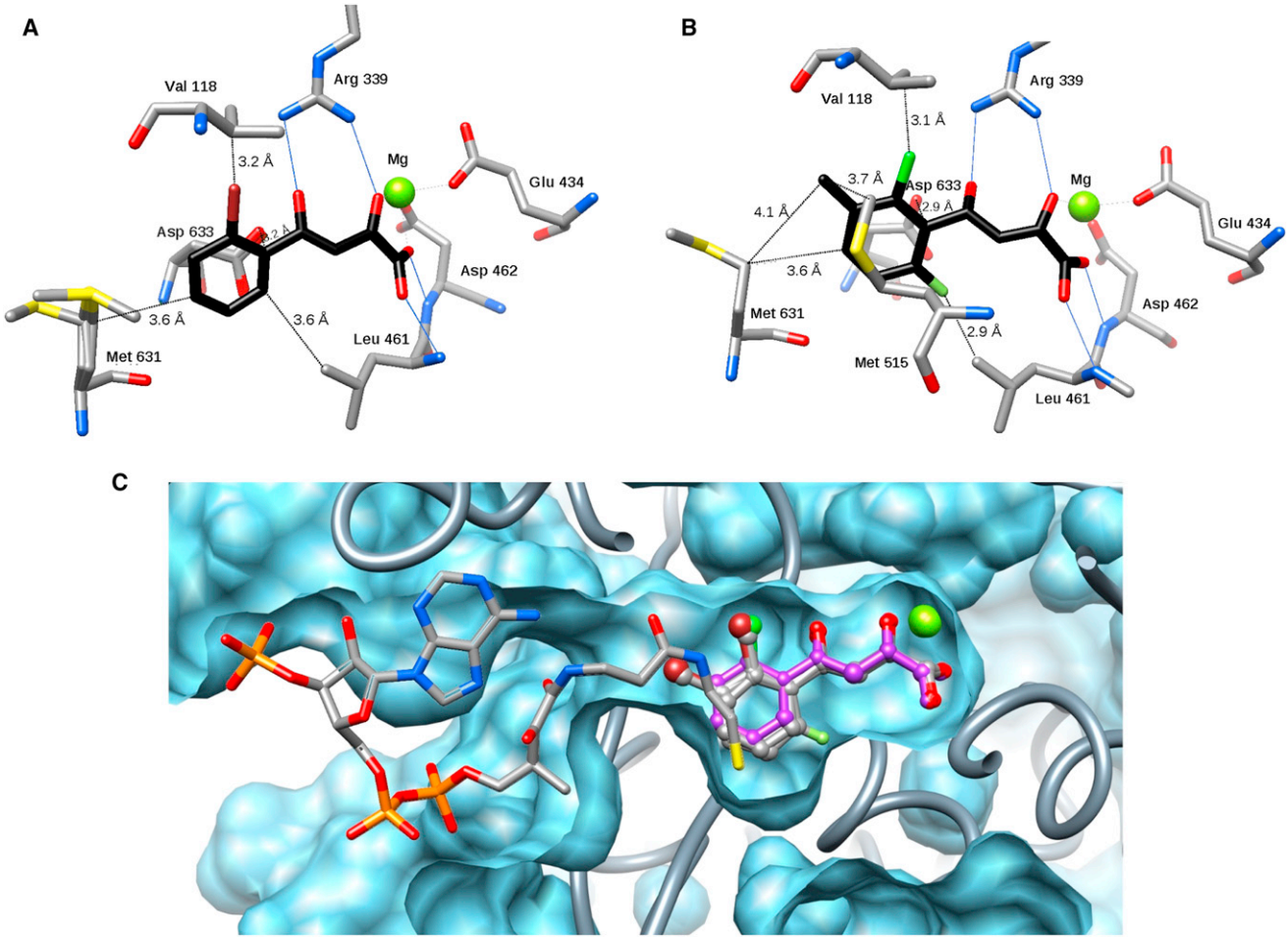

Figure 3. Comparing Binding of PDKA Analogs to GlcB

(A and B) Binding of GlcB to inhibitor **4** (A) and inhibitor **11** (B) colored by element, with $C_{protein}$ in gray and C_{ligand} in black. Hydrogen bonds are indicated by solid blue lines, and distances from key positions on the phenyl ring to protein residues are marked as dashed lines.

(C) Crystal structure overlay of GlcB complexed with PDKA (in magenta); **1**, **4**, **7**, and **11**, represented by ball-and-stick, and CoA, represented by a stick model (colored by element), with the Mg atom in green, illustrate the relative positions of the ligands occupying the active site channel (presented by protein surface calculated in CHIMERA (Pettersen et al., 2004). The CoA model and protein surface were made from chain A of the 2GQ3 model.

See also Figure S3.

in vivo testing, we chose to pursue compounds with two substitutions. Trisubstituted 2-Cl-6-F-3-Me-PDKA (**11**) did not result in an additive affinity of each position (IC_{50} = 5.5 μM). However, **11** proved to be a good candidate for future study, as its methyl ester derivative exhibited a good combination of essential features (reasonable potency, high bioavailability, low toxicity) to test for efficacy in an animal model of TB infection.

Antimycobacterial Activity of PDKA Inhibitors

We carried out whole-cell testing of growth inhibition by PDKAs on 0.2% acetate-supplemented M9 media to model fatty acid-driven metabolism and 0.2% dextrose-supplemented 7H9 media to model carbohydrate-oriented metabolism for comparison. Initial testing was conducted with a Biosafety Level 2 (BL2)-approved vaccine strain of *Mtb* with deletions of the *panCD* genes and the RD1 region (mc^2-7000) (Sambandamurthy et al., 2006). Freshly synthesized inhibitors were solubilized immediately prior to MIC determination (presented in Tables 1 and 3). Almost all of the PDKA inhibitors with reasonable potency against the enzyme inhibited growth of bacteria on acetate. Furthermore, they were less potent on carbohydrate (dextrose), with MICs usually 2- to 4-fold higher than on acetate, suggesting that they affect the glyoxylate shunt. In the context of this article, MICs are reported as MIC_{99}, which refers to the minimum concentration of a compound at which bacteria growth is inhibited by >99%, as assessed by absence of respiration in the rezasurin (AlamarBlue) assay. Testing on other tuberculosis strains and clinical isolates has not yet been carried out.

To improve whole-cell activity, we used a prodrug strategy by masking the acid via esterification as a way to enhance cellular uptake. Simple alkyl esters of whole-cell-active PDKA analogs had approximately 8-fold lower MICs compared to their corresponding PDKAs (Table 3). Of particular interest were the ester prodrugs of the *ortho*-bromo (**4**), *ortho*-methyl (**5**), and

Table 3. H37Rv Activity, Mouse Plasma Protein Binding, and Mouse Microsomes Clearance Data for Alkyl- and Benzyl-ester Prodrugs of Selected PDKA Analogs

Compound	H37Rv MIC_{99} on Acetate (μM)	H37Rv MIC_{99} on Dextrose (μM)	Mouse Microsomes Clearance (ml/min/g)	Mouse Plasma Protein Binding (%)
11	16	32	<0.3	70 ± 3.0
Me ester of **11** (**12**)	2	8	0.6 ± 0.2	91.9 ± 1.6
Benzyl ester of **11**	<1	2	>30	ND
4	16	32	<0.3	67.5 ± 2.6
Me ester of **4**	8	16	3.2 ± 0.7	87.7 ± 1.6
Benzyl ester of **4**	<1	8	15.3 ± 6.1	ND
1	16	32	ND	70.7 ± 1.8
Me ester of **1**	4	16	4.6 ± 0.7	87.1 ± 1.4
Benzyl ester of **1**	<1	16	>30	ND

See also Tables S1 and S3.

2-chloro-6-fluoro-3-methyl (**11**) PDKAs. These exhibited MIC values in the ≤1 to 8 μM range against H37Rv grown on acetate as a carbon source (Table 3). In agreement with earlier data on the *Mtb* mc^2-7000 strain, PDKA esters inhibited growth of the H37Rv strain on dextrose-supplemented media with 2- to 4-fold higher MICs. In addition, Caco-2 uptake studies (Yazdanian et al., 1998) demonstrated the enhanced permeability of esters compared to their corresponding acids. Permeability ranged from a nondetectable level for acid **11** to a high level of 371 nm/s for the corresponding methyl ester **12**). This suggests they could potentially be orally bioavailable and taken up through the gut. Following the decomposition of the benzyl- and methyl esters of **11** in whole-cell lysates over time by MS demonstrated accumulation of acid **11** and no other product (Table S2). As expected, none of the PDKA esters themselves were directly active against GlcB in the enzyme assay. However, upon hydrolysis with longer preincubation, each ester decomposed to yield the parent PDKA (free acid) active against the enzyme. Furthermore, PDKA esters inhibited malate synthase activity in mycobacterial cell lysates (Tables S1 and S2). These compounds achieved IC_{50}s in whole-cell lysates similar to the purified enzyme assay. No loss of inhibition was observed even after 3 hr of incubation due to potential reactivity or binding to other proteins. This argues that these compounds act on GlcB inside the cell (Table S1).

The methyl ester of **11** (**12**) was tested using the standard minimal bactericidal concentration (MBC) determination protocol (Motyl et al., 2006). It was shown to be bactericidal to mc^2-7000 in culture on either acetate or dextrose carbon sources. The MBC was approximately the same as the MIC when grown on acetate. The MBC was 2- to 4-fold higher than the MIC on dextrose. Compound **12** was also tested in the Low-Oxygen Recovery Assay (LORA) and was found active against H37Rv grown on dextrose (MIC = 52 μM). LORA is one of the in vitro models of the nonreplicating drug-tolerant state of *Mtb* (Cho et al., 2007). The observed 4- to 5-fold shift of MIC in the LORA assay compared to the MABA assay (Microplate Alamar Blue Assay; Franzblau et al., 1998) (MIC = 11 μM) is consistent with what has been observed for other antitubercular drugs with activity against nonreplicating bacteria, such as rifampicin (Cho et al., 2007).

To confirm that GlcB is the intracellular target responsible for growth inhibition in *Mtb*, we constructed a GlcB-overexpressing strain in *Mtb* containing a plasmid with either GlcB under a tetracycline-inducible promoter or an unrelated *Mtb* protein (Rv3547) as a control. An 8-fold increase in the MIC for **12** (12.5 to 100 μM) was observed after induction of GlcB expression using anhydrotetracycline on M9 media with acetate. A 4-fold increase in the MIC (25 to 100 μM) was observed on 7H9-dextrose. In contrast, the strain with the control plasmid (Rv3547) showed no shift in MIC for compound **12**. All strains displayed the same MIC for rifampicin (with or without anhydrotetracycline) as the untransformed parental strain. The observed increase in the MIC for compound **12** in response to GlcB overexpression strongly supports on-target activity. In addition, we have tested PDKA inhibitors (**4** and **11**) at a high concentration of 100 μM on four purified enzymes in the core metabolic pathways from *Mtb* which react with similar substrates (ICL, phosphoenolpyruvate carboxykinase, isocitrate dehydrogenase, and pyruvate kinase) and observed no inhibition (data not shown). This adds to reassurance that inhibition is specific to GlcB.

Inhibition of GlcB in a Murine Model of TB

We evaluated the pharmacologic properties of several of the most potent inhibitors and selected a representative for evaluation in a mouse model of TB infection. The most important factors we considered were solubility, chemical stability, plasma protein binding, serum stability, metabolic clearance in microsomes, and pharmacokinetic profile. The ADME (absorption, distribution, metabolism, excretion) guidelines we used were: solubility in PBS at >20 μg/ml, stability in human and murine plasma >70% over 1 hr, clearance in mouse microsomes after 30 min < 15 ml/min/kg, and Caco-2 permeability > 100 nm/s. The methyl ester **12** showed the best combination of potency with in vitro PK properties among the PDKA analogs tested (Table 3) and, therefore, was selected for further in vivo PK, PD, and toxicity studies. In mice, **12** was orally bioavailable (%F = 92) and attained sufficient blood levels (i.e., at 600 mg/kg dosing: T_{max} = 0.25 hr, C_{max} = 99.5 μg/ml, and $AUC_{8\ hr}$ = 54.3 μg × hr/ml). **12** demonstrated good stability in CD1 mouse plasma, exhibiting slow hydrolysis of the ester to yield the parent PDKA derivative ($t_{1/2}$ = 30 min, conversion from **12** to **11** in plasma). The

Table 4. Therapeutic Efficacy of 12 against *Mtb* in Mice

Compound	Target Dose (mg/kg)	Experimental Dose (mg/kg)	Administration (per day)	Decrease in $\log_{10}$ CFU in Lungs[a]	SE
Moxifloxacin	30	36	Once	3.07	0.064
12	500	542	Once	1.68	0.103
12	600	718	Once	1.72	0.149
12	300	377	Twice	1.89	0.079
12	400	460	Twice	2.12	0.108

Five animals in each testing group were inoculated with 10^5 CFU of *Mtb* intratracheally, and treatment started 1 day postinfection. Nine days postinfection, the mice were sacrificed, and the respective bacterial loads in the lungs were determined.
See also Figure S4.
[a]All reductions in CFU were statistically significant over the untreated control group by a t test (df = 9,10; $p < 0.0001$).

corresponding acid, **11**, demonstrated a low rate of clearance in a mouse liver microsome assay (<0.3 ml/min × g), and a reasonable level of mouse plasma protein binding (70%). (The eventual disposition of **11**, whether by metabolism or excretion, was not determined in vivo.) The achieved exposure for **12** in mice, as measured by $AUC_{free}/MIC_{H37Rv/acetate}$ (35 at 600 mg/kg oral dosing), compared reasonably well to clinical antituberculars such as moxifloxacin ($AUC_{free}/MIC_{H37Rv/acetate}$ = 142 at 100 mg/kg oral dosing). (PK curves for **12** and its activated form **11** are shown in Figure S4.) The PK data show that the peak blood concentration achieved for compound **12** at 300, 500, and 600 mg/kg was approximately 150- to 200-fold higher than the MIC for H37Rv (2 μM = 0.548 μg/ml). The exposure was maintained above the MIC value for at least 6–7 hr. Assessment in C57BL/6J mice with a single-dose oral administration of **12** formulated in Solutol (30%) and PEG 400 (70%) demonstrated that a dose of 1,000 mg/kg (the highest tested) was not lethal. The maximum tolerated dose (MTD) was determined to be 600 mg/kg. No toxicity effects were observed at 400 mg/kg p.o. twice daily.

Compound **12** was tested in a murine model of acute TB infection (Rullas et al., 2010). C57BL/6J mice were infected intratracheally with 10^5 colony-forming units (CFU) and treated for 9 days, followed by determination of bacillary load in the lungs. Several dosing strategies from 300 to 600 mg/kg were tested to determine the best compound exposure above the MIC at or below the MTD established. Treatment with moxifloxacin (30 mg/kg), which is used in the treatment of multidrug-resistant tuberculosis (Cox et al., 2011), was used for comparison. At all dosing levels (once daily [u.i.d.] and twice daily [b.i.d.]), **12** exhibited a statistically significant reduction (p values < 0.0001) in the *Mtb* bacterial load compared to the control (Table 4). In fact, at 400 mg/kg b.i.d. dosing, **12** reduced the bacterial load by over 100-fold ($\Delta\log_{10}$ CFU = 2.12), within an order of magnitude of moxifloxacin ($\Delta\log_{10}$ CFU = 3.07). This activity was achieved despite the fact that the dosage, which was limited by the MTD, provided exposure well above the MIC for only 6–8 hr at a time. Thus, inhibition of GlcB resulted in impairment of the ability to establish an acute infection in mice, similar to the results obtained with a Δ*icl1/2* strain (Muñoz-Elías and McKinney, 2005).

DISCUSSION

Our studies have shown that malate synthase is essential for *Mtb* survival both in vitro and in vivo, and this enzyme can be targeted with PDKA inhibitors. Structure-guided design led to the identification of highly potent inhibitors, some with submicromolar IC_{50}s. While the acids in the series displayed difficulty penetrating the cell wall, esters of these compounds acted as prodrugs that could be taken up and hydrolyzed inside cells, leading to potent growth inhibition. Overexpression of the enzyme leads to a 4–8-fold increase in MIC for these compounds—evidence that GlcB is the target whose inhibition is responsible for cell death. Furthermore, we observed a correlation in structure–activity relationship, where analogs with different substituents around the PDKA core that inhibit the enzyme (or their corresponding esters) also inhibit whole-cell growth, and analogs with substituents that abrogate activity against the enzyme are also inactive against whole cells. This correlation of SAR would be highly improbable if the actual target of these compounds inside the cell were an enzyme other than GlcB. Finally, the compounds are consistently 4-fold more potent in cultures grown on acetate as a carbon source compared to dextrose conditions. Based on these observations, we conclude that inhibition of GlcB is the mechanism of action of the PDKAs in vivo.

The observation that inhibitors of GlcB are bactericidal for *Mtb* grown on carbon sources other than fatty acids, such as carbohydrates like dextrose, was unexpected because inactivation of ICL is tolerated when grown in vitro on carbohydrates (McKinney et al., 2000). Since ICL2 also has partial isocitrate lyase activity (Gould et al., 2006), a Δ*icl1/icl2* double mutant of *Mtb* completely lacking a functional glyoxylate shunt was constructed and was also found to be able to grow on dextrose (Muñoz-Elías and McKinney, 2005). However, the Δ*icl1/icl2* double mutant grew at a suppressed rate (2- to 4-day lag), suggesting that the glyoxylate shunt might be playing a metabolic role even when *Mtb* is growing on carbohydrates. Unlike *E. coli* and other well-studied bacteria, which suppress anaplerosis in the presence of a preferred carbon source like carbohydrates (Fischer and Sauer, 2003), *Mtb* catabolizes carbohydrates and fatty acids concurrently in vitro with no apparent repression (de Carvalho et al., 2010). Supporting the observation that GlcB is essential in vitro, recent high-density transposon-mutagenesis experiments have shown that *glcB* is essential for growth on glycerol as well as cholesterol as a carbon source (Griffin et al., 2011).

One possible explanation for the requirement for GlcB could be to avoid accumulation of glyoxylate. Glyoxylate has been shown to be toxic in other bacteria (Nuñez et al., 2001). However, *Mtb* is able to grow on glyoxylate as a sole carbon source (our

unpublished data). Furthermore, there are other enzymes (i.e., glycine dehydrogenase or glyoxylate aminotransferase) that can utilize glyoxylate as a substrate (Sakuraba et al., 2008; Wayne and Lin, 1982). In addition, we found, that, when the ICL inhibitor 3-nitropropionate (3-NP) is coadministered at a low sub-MIC concentration (20 μM) with GlcB inhibitors to *Mtb* cultures grown on 7H9-dextrose media, it causes a decrease in MIC (e.g., from 12.5 μM to 1.56 μM for **12**). In theory, the presence of 3-NP should reduce glyoxylate accumulation by suppressing flux through the glyoxylate shunt and would thus be expected to cause an increase in MIC for GlcB inhibitors. The decrease in MIC we observed suggests that the requirement for GlcB in vitro under carbohydrate-supplemented growth conditions might not be limited to a need for glyoxylate detoxification.

There are several alternative reasons why GlcB inhibition under carbohydrate-supplemented growth conditions might result in cell death. Functional GlcB might be required when grown on dextrose to replenish the intermediates on the reductive side of TCA cycle (succinate, malate, and oxaloacetate). These were shown to be maintained at relatively low intracellular concentrations by metabolite tracing (de Carvalho et al., 2010). A recent analysis of ^{13}C metabolic flux in *Mtb* demonstrated a constant flux through the glyoxylate shunt, even with glycerol as a carbon source. Furthermore, disruption of *icl1* resulted in a loss of viability at a slow growth rate (Beste et al., 2011). This echoes the finding of ICL1's importance to *Mtb*'s ability to adapt to nutrient-limiting conditions by regulating ATP levels required for entering a nonreplicating state (Gengenbacher et al., 2010). These data point to the conclusion that the role of the glyoxylate shunt extends beyond its anaplerotic function in *Mtb*. Despite the uncertainty about its metabolic role under carbohydrate-supported growth conditions, our results make it clear that inhibition of GlcB is lethal to *Mtb* grown on multiple carbon sources, and this provides a route to antitubercular drug development.

SIGNIFICANCE

Novel enzyme targets are needed to drive discovery of new drugs for combating tuberculosis. Because of its role in the glyoxylate shunt, we have investigated malate synthase (GlcB) as an attractive target and identified a series of potent inhibitors with a phenyl-diketo acid (PDKA) scaffold. A selected compound (12) in the PDKA series was shown to have efficacy in a mouse model of infection. While complete sterilization was not achieved, the bacterial load was reduced nearly 100-fold over the course of 9 days. It is interesting that the compound appears to be active during the acute phase of infection, which is consistent with the essential role of GlcB for growth on other carbon sources in addition to fatty acids. Thus, these compounds have the potential to have activity during both acute and chronic phases of infection. It is likely that with further optimization, a more potent compound than 12 (which was chosen for a tradeoff of pharmacokinetic/pharmacodynamic properties) would be able to achieve even higher bacterial clearance in vivo. Nonetheless, the statistically significant reduction of the bacterial load observed indicates that the PDKA compounds could have therapeutic potential and provides evidence that *Mtb* GlcB could be a clinically relevant target. These structural studies will form the foundation for development of better GlcB inhibitors to be used eventually in human clinical trials.

EXPERIMENTAL PROCEDURES

Protein Overexpression and Purification

GlcB with the Cys619 mutated to Ala was cloned into a custom vector *p6HisF-11d,* expressed in *E. coli* BL21 cells, and purified by Ni affinity and size exclusion columns as described previously (Smith et al., 2003). As the presence of the His-tag did not change the results of the enzyme assay or crystallization, most of the reported work was done using GlcB with the N-terminal His-tag intact.

DTNB-Coupled Enzyme Assay

For the C619A GlcB mutant enzyme, a DTNB-coupled assay was used to evaluate inhibition activity. A BMG POLARstar OPTIMA plate reader was used to determine the inhibition of GlcB by continuously monitoring the formation of CoA in the forward enzymatic reaction by the increase in absorbance at 412 nm due to 5,5′-dithiobis-(2-nitrobenzoic acid) (DTNB)-CoA adduct formation, over a period of 20 min. The 96-well plates contained 100 μl total reaction volume with 13 nM C619A GlcB in the reaction buffer (20 mM Tris, pH 7.5, and 5 mM $MgCl_2$). All inhibitors (in 100% DMSO) were added such that the final reaction mixture contained 1% DMSO. Inhibitors were incubated with GlcB in the reaction buffer for 20 min at room temperature before adding 0.6 mM acetyl-CoA. The reaction was initiated by the addition of 1.2 mM glyoxylate and 0.5 mM (final concentration) DTNB. Each data point for the IC_{50} plots was measured in triplicate. The data reported in this article reflect the most robust enzyme assay conditions. We noticed that a longer preincubation time with GlcB (probed up to 3 hr), and lower Mg^{2+} concentrations in the assay buffer (1–5 mM, still in vast excess to the K_M for this metal ion as a cofactor in the reaction) led to enhanced enzyme inhibition for the PDKA family of inhibitors (relative to control reactions of the enzyme incubated for the same duration, in the same Mg^{2+} concentrations without inhibitor in each case, which corrects for the slight loss of activity of the enzyme over time due to protein instability). It appears that PDKA inhibitors are slow to reach equilibrium binding, probably because they bind through chelating Mg^{2+} in the same manner as glyoxylate (Copeland, 2005). However, incubating longer than 30 min at room temperature led to a decrease in enzyme velocity and reduced assay reproducibility and was not done for routine inhibitor testing aiming at building SAR.

Pyruvate-Dehydrogenase-Coupled Assay

For the wild-type GlcB enzyme, this assay was used because the Cys619 in the active site is sensitive to oxidation by the DTNB in the coupled reaction. Velocity was measured by monitoring the increase of fluorescence (excitation at 340 nm, emission at 480 nm) due to NADH production coupled with the release of CoA. Final concentrations in the reaction mixture were: 3 nM of GlcB, 0.1 Ul/ml of pyruvate dehydrogenase (PDH), 50 μM glyoxylate, 2 μM acetyl CoA, 500 μM NAD, 500 μM pyruvate, 200 μM thiamine pyrophosphate, 5 mM $MgCl_2$, 0.8 mM EDTA, 50 mM Tricine pH 7.4. EDTA was included in the assay buffer in both assays because it enhances the stability of the enzyme and does not affect the enzyme velocity, although it is over 6-fold lower than the concentration of Mg^{2+} used. The same assay was used in mycobacterial cell lysate (1 mg/ml total protein concentration measured by Bradford assay), with cells harvested at midlog phase and disrupted by sonication.

Inhibitor Synthesis

Chemical syntheses of the PDKA compounds used in this study are described in the Supplemental Information. Chemical structures for compounds **1–12** are shown in Figure S5.

Protein Crystallization, Data Collection, and Data Analysis

Purified C619A GlcB (with His_6 tag) at a concentration of 5 mg/ml in 20 mM Tris-HCl, pH 7.5, buffer with 0.1 M NaCl was mixed for crystallization with an equal volume of mother liquor of 18%–22% PEG 3350, 0.1 M $MgCl_2$, and 0.1 M Tris-HCl, pH 8.0. Crystals were obtained by hanging drop vapor diffusion

within 2–3 weeks. Inhibitors were soaked in by transferring preformed GlcB crystals into a drop made from mother liquor with 1–5 mM of inhibitor added from a DMSO stock solution such that the final DMSO concentration was below 1%, and incubated for 1–5 days. Prior to data collection crystals were cryo-protected by Fomblin (Sigma) and flash frozen in liquid nitrogen. Data were collected at Argonne National Lab APS synchrotron, beamlines 19- and 23-ID, at 0.98 Å. Diffraction data were indexed, integrated, and scaled in HKL2000 (Otwinowski and Minor, 1997). Data were truncated in Collaborative Computational Project, Number 4 (1994). 1N8I (Smith et al., 2003) with only the protein atoms included in the refinement was used as the model for the initial rigid body refinement of the isomorphous $P4_32_12$ crystal in REFMAC (Murshudov et al., 2011). Then iterative runs of inspection and manual modification in COOT (Emsley et al., 2010) and refinement in PHENIX (Adams et al., 2002) with simulated annealing were done to gradually improve the model. The ligand model and dictionary files were created in ELBOW BUILDER from the PHENIX suite and fitted into the density in COOT. Final refinement was done in BUSTER, Version 2.9. For data collection and refinement statistics see Table 2. All ligands had strong electron density in the 2Fo-Fc map covering all atoms visible (see example shown in Figure S2). After refinement, the halogens in halogen-containing inhibitors displayed negative Fo-Fc peaks over them in the Fourier difference map. This might have been an artifact due to radiation damage, as refinement with data truncated to very low-redundancy reflections showed no negative Fo-Fc density at these sites. For final model refinement, high redundancy sets were used, and individual occupancies were refined for halogen-containing ligands to eliminate disagreement in the Fo-Fc map. Ramachandran statistics are as follows (given in order most favored/additionally favored regions/outliers in percentage): GlcB-PDKA, 97.11/2.02/0.87; GlcB-**4**, 97.21/1.76/0.73; GlcB-**1**, 97.34/2.22/0.44; GlcB-**7**, 97.27/2.16/0.58; and GlcB-**11**, 96.85/3.01/0.14. All of the Ramachandran outliers are on the surface of the protein except Glu273, which hydrogen bonds with a water molecule coordinating the Mg^{2+}. This unusual backbone conformation is well supported by the electron density in all data sets.

Whole-Cell Testing

MIC determination was done using the MABA (Franzblau et al., 1998) assay in 96-well plates. For the *Mtb* mc^2-7000 strain (Sambandamurthy et al., 2006), cells were grown in 7H9 media with OADC supplement (Middlebrook), 0.05% Tyloxapol (Sigma), and 25 μg/ml pantothenate to an optical density 600 (OD_{600}) of 1–2. Then cells were diluted into testing media to an OD_{600} of 0.01 and pipetted into testing plates, 200 μl per well. The two testing media were: 7H9 media with 0.2% dextrose, 0.085% NaCl, 0.05% Tyloxapol, and 25 μg/ml pantothenate or M9 (Sigma) media with 0.25% sodium acetate, 2 mM $MgSO_4$, 0.1 mM $CaCl_2$, 0.05% Tyloxapol, and 25 μg/ml pantothenate. Then each compound was added as a 1/2 serial dilution in DMSO (2% DMSO final in a well). 7H9-dextrose plates were incubated for 6 days before staining with resazurin (Sigma), and M9-acetate plates were incubated for 3 weeks and then for an additional 2 days after staining at 37°C with shaking. The lowest concentration where resazurin stayed completely unconverted was recorded as the MIC_{99} value. MIC_{99} refers to the minimum concentration at which growth of the experimental strain mc^2-7000 is inhibited by >99%, as assessed by absence of respiration in the rezasurin (AlamarBlue) assay. Rifampicin was used as a control: for mc^2-7000 *Mtb* displaying an MIC_{99} of 0.125 μM in 7H9-dextrose, and an MIC_{99} of 0.25 μM in M9-acetate. MIC values for rifampicin varied no more than one dilution point from run to run. All MIC_{99} values reported are overage with 1/2 dilution precision from at least three independent experiments. For H37Rv *Mtb* strain testing, an inoculum standardized to approximately 1×10^7 CFU × ml^{-1} was diluted 1 in 200 in testing media of 7H9, ADC, 0.025% Tween 80, 0.085% NaCl or 7H9, 0.5% albumin, 0.1% sodium acetate, 0.025% Tween 80, 0.085% NaCl. Inhibitors were tested as with the mc^2-7000 strain. Plates were incubated at 37°C for 6 days before and 24–48 hr after staining with resazurin.

Mouse Microsome Clearance and Plasma Protein Binding

Microsomal intrinsic clearance was measured as described by (Clarke and Jeffrey, 2001). The compound (0.5 μM) was incubated with 0.5 mg/ml microsomal protein, 0.34 mg/ml NADP, 1.56 mg/ml glucose-6-phosphate, and 1.2 U/ml glucose-6-phosphate dehydrogenase, 2.6 mg/ml UDPGA, 0.5% (v/v) methanol in 50 mM potassium phosphate buffer, pH 7.4, at 37°C. Fifty microliter aliquots of the incubation mixture were withdrawn at various time points over 30 min and added to 100 ml stop solution (80:20:1 (v/v/v) acetonitrile:ethanol:acetic acid) containing internal standard. Samples were snap frozen and stored at −80°C until analyzed by liquid chromatography/tandem mass spectrometry (LC/MS/MS). Prior to analysis, samples were thawed at room temperature, vortexed, and then centrifuged, and the supernatant was taken for analysis. No cofactor controls were included to assess non-P450 dependent clearance. Clearance was estimated for midazolam in parallel to assure integrity of the microsomal preparations and acceptable interassay variability. The intrinsic clearance was calculated based on the method published by (Obach et al., 1997), using the first-order elimination rate constant for disappearance of the parent compound. This was calculated from the slope of the log-transformed concentration-time curve using SigmaPlot 8.0 (Systat Software). Clearances were expressed in milliliters per minute per gram of liver. The clearance was predicted based on the assumption that the drug concentration (0.5 μM) was most likely well below the K_M. The lower limit of quantification was 0.5 ml/min/g liver, and this corresponded to a <15% decrease in the parent compound in 30 min. The in vitro plasma protein binding of the diketo acids was determined by equilibrium dialysis (three cells per species) in fresh mouse and human plasma at 0.5 and 5 mg/ml (0.5% [v/v] DMSO final concentration). Spiked plasma samples were mixed gently, and triplicate aliquots were collected to verify initial concentrations. Following assembly of dialysis rapid equilibrium devices (RED) (Thermo Scientific) (molecular weight cutoff limit of 8,000–10,000 Da), spiked plasma was placed in the donor compartment of the cell and PBS, pH 7.4, in the receiver compartment. Cells were incubated in a water bath at 37°C and mixed continuously for 6 hr. Triplicate aliquots (volume determined gravimetrically) from donor and receiver compartments were snap frozen and stored at −30°C prior to analysis. Percent binding was estimated using standard equations which accounted for volume changes due to Donnan effects (Boudinot and Jusko, 1984).

Pharmacokinetic Measurement

The compound was assayed as a single oral dose at 20 mg/kg, 100 mg/kg, and 600 mg/kg in female C57BL/6J mice, dissolved in PEG 400/Solutol 70:30. The sampling scheme postadministration was 15, 30, and 45 min, respectively, at 1, 1.5, 2, 3, 4, and 8 hr; four animals per time point. Peripheral blood levels were analyzed by LC/MS/MS. Data analysis was performed with WinNonlin 5.2; noncompartmental analysis (NCA).

Efficacy in Mouse Model of TB

To assess the therapeutic efficacy of compound **12** against *M. tuberculosis* in an acute murine model of intratracheal infection (Rullas et al., 2010), mice were infected with 10^5 CFU and lung homogenates were obtained 9 days after infection (n = 4–5 mice per group for all groups). Compound **12** was administered according to the schedule indicated in Table 4 (either once a day or twice a day) using PEG 400/Solutol 70:30 as the vehicle. Moxifloxacin (30 mg/kg) dissolved in Captisol 20% was used as quality control of the assay and reduced the CFU lung number by 3.07 logs with respect to untreated mice. The average log CFU in the lungs of untreated mice was 7.13. All mice experiments were done in compliance with GSK regulations.

ACCESSION NUMBERS

Crystal structures of GlcB in complex with inhibitors were deposited in the Protein Data Bank under entry IDs 3S9I, 3S9Z, 3SAD, 3SAZ, and 3SB0.

SUPPLEMENTAL INFORMATION

Supplemental Information includes Supplemental Experimental Procedures, two tables, and five figures and can be found with this article online at http://dx.doi.org/10.1016/j.chembiol.2012.09.018.

ACKNOWLEDGMENTS

The authors thank Dr. S.G. Franzblau for testing **12** in the LORA assay; Hongye Li for cloning GlcB into PDT vector; the TAMU chemistry group, currently led by

Dr. N. Zhou, for synthesizing ~400 compounds for this project; Tracey Musa for comments on the manuscript; and the GSK team: Dr. F. Ortega, for conducting PK experiments; A. Santos-Villarejo, for plasma protein binding and stability experiments; Dr. J. Trullas, for in vivo efficacy experiments; D. Alvarez-Gomez, for wild-type enzyme testing, and Dr. E. Perez-Herranz, for whole-cell H37Rv testing.

This work was funded by grants to J.C.S.: Grant A-0015 from the Welch Foundation, National Institutes of Health Grant P01 AIO 68135, and the Global Alliance for TB Drug Development. Data were collected at Argonne National Laboratory, beamlines 19ID and 23ID.

Received: July 11, 2012
Revised: September 14, 2012
Accepted: September 19, 2012
Published: December 20, 2012

REFERENCES

Adams, P.D., Grosse-Kunstleve, R.W., Hung, L.W., Ioerger, T.R., McCoy, A.J., Moriarty, N.W., Read, R.J., Sacchettini, J.C., Sauter, N.K., and Terwilliger, T.C. (2002). PHENIX: building new software for automated crystallographic structure determination. Acta Crystallogr. D Biol. Crystallogr. *58*, 1948–1954.

Adams, R. July 2008. Certain pyrazoline derivatives with kinase inhibitory activity. U.S. patent 2,007,026,034.

Anstrom, D.M., and Remington, S.J. (2006). The product complex of M. tuberculosis malate synthase revisited. Protein Sci. *15*, 2002–2007.

Anstrom, D.M., Kallio, K., and Remington, S.J. (2003). Structure of the Escherichia coli malate synthase G:pyruvate:acetyl-coenzyme A abortive ternary complex at 1.95 A resolution. Protein Sci. *12*, 1822–1832.

Berryman, O.B., Bryantsev, V.S., Stay, D.P., Johnson, D.W., and Hay, B.P. (2007). Structural criteria for the design of anion receptors: the interaction of halides with electron-deficient arenes. J. Am. Chem. Soc. *129*, 48–58.

Beste, D.J.V., Bonde, B., Hawkins, N., Ward, J.L., Beale, M.H., Noack, S., Nöh, K., Kruger, N.J., Ratcliffe, R.G., and McFadden, J. (2011). ^{13}C metabolic flux analysis identifies an unusual route for pyruvate dissimilation in mycobacteria which requires isocitrate lyase and carbon dioxide fixation. PLoS Pathog. *7*, e1002091.

Bloch, H., and Segal, W. (1956). Biochemical differentiation of Mycobacterium tuberculosis grown in vivo and in vitro. J. Bacteriol. *72*, 132–141.

Boudinot, F.D., and Jusko, W.J. (1984). Fluid shifts and other factors affecting plasma protein binding of prednisolone by equilibrium dialysis. J. Pharm. Sci. *73*, 774–780.

Cho, S.H., Warit, S., Wan, B., Hwang, C.H., Pauli, G.F., and Franzblau, S.G. (2007). Low-oxygen-recovery assay for high-throughput screening of compounds against nonreplicating Mycobacterium tuberculosis. Antimicrob. Agents Chemother. *51*, 1380–1385.

Clark, J.D., O'Keefe, S.J., and Knowles, J.R. (1988). Malate synthase: proof of a stepwise Claisen condensation using the double-isotope fractionation test. Biochemistry *27*, 5961–5971.

Clarke, S.E., and Jeffrey, P. (2001). Utility of metabolic stability screening: comparison of in vitro and in vivo clearance. Xenobiotica *31*, 591–598.

Collaborative Computational Project, Number 4. (1994). The CCP4 suite: programs for protein crystallography. Acta Crystallogr. D Biol. Crystallogr. *50*, 760–763.

Copeland, R.A. (2005). Evaluation of enzyme inhibitors in drug discovery. A guide for medicinal chemists and pharmacologists. Methods Biochem. Anal. *46*, 1–265.

Cox, H., Ford, N., Keshavjee, S., McDermid, C., von Schoen-Angerer, T., Mitnick, C., and Goemaere, E. (2011). Rational use of moxifloxacin for tuberculosis treatment. Lancet Infect. Dis. *11*, 259–260.

de Carvalho, L.P.S., Fischer, S.M., Marrero, J., Nathan, C., Ehrt, S., and Rhee, K.Y. (2010). Metabolomics of Mycobacterium tuberculosis reveals compartmentalized co-catabolism of carbon substrates. Chem. Biol. *17*, 1122–1131.

Dunn, M.F., Ramírez-Trujillo, J.A., and Hernández-Lucas, I. (2009). Major roles of isocitrate lyase and malate synthase in bacterial and fungal pathogenesis. Microbiology *155*, 3166–3175.

Egbertson, M.S. (2007). HIV integrase inhibitors: from diketoacids to heterocyclic templates: a history of HIV integrase medicinal chemistry at Merck West Point and Merck Rome (IRBM). Curr. Top. Med. Chem. *7*, 1251–1272.

Emsley, P., Lohkamp, B., Scott, W.G., and Cowtan, K. (2010). Features and development of Coot. Acta Crystallogr. D Biol. Crystallogr. *66*, 486–501.

Fischer, E., and Sauer, U. (2003). A novel metabolic cycle catalyzes glucose oxidation and anaplerosis in hungry *Escherichia coli*. J. Biol. Chem. *278*, 46446–46451.

Franzblau, S.G., Witzig, R.S., McLaughlin, J.C., Torres, P., Madico, G., Hernandez, A., Degnan, M.T., Cook, M.B., Quenzer, V.K., Ferguson, R.M., and Gilman, R.H. (1998). Rapid, low-technology MIC determination with clinical Mycobacterium tuberculosis isolates by using the microplate Alamar Blue assay. J. Clin. Microbiol. *36*, 362–366.

Gengenbacher, M., Rao, S.P.S., Pethe, K., and Dick, T. (2010). Nutrient-starved, non-replicating Mycobacterium tuberculosis requires respiration, ATP synthase and isocitrate lyase for maintenance of ATP homeostasis and viability. Microbiology *156*, 81–87.

Gould, T.A., van de Langemheen, H., Muñoz-Elías, E.J., McKinney, J.D., and Sacchettini, J.C. (2006). Dual role of isocitrate lyase 1 in the glyoxylate and methylcitrate cycles in Mycobacterium tuberculosis. Mol. Microbiol. *61*, 940–947.

Griffin, J.E., Gawronski, J.D., Dejesus, M.A., Ioerger, T.R., Akerley, B.J., and Sassetti, C.M. (2011). High-resolution phenotypic profiling defines genes essential for mycobacterial growth and cholesterol catabolism. PLoS Pathog. *7*, e1002251.

Jackson, M.R., Beahm, R., Duvvuru, S., Narasimhan, C., Wu, J., Wang, H.-N., Philip, V.M., Hinde, R.J., and Howell, E.E. (2007). A preference for edgewise interactions between aromatic rings and carboxylate anions: the biological relevance of anion-quadrupole interactions. J. Phys. Chem. B *111*, 8242–8249.

Kornberg, H.L., and Krebs, H.A. (1957). Synthesis of cell constituents from C2-units by a modified tricarboxylic acid cycle. Nature *179*, 988–991.

Laskowski, R.A., and Swindells, M.B. (2011). LigPlot+: multiple ligand-protein interaction diagrams for drug discovery. J. Chem. Inf. Model. *51*, 2778–2786.

Lorenz, M.C., and Fink, G.R. (2001). The glyoxylate cycle is required for fungal virulence. Nature *412*, 83–86.

McKinney, J.D., Höner zu Bentrup, K., Muñoz-Elías, E.J., Miczak, A., Chen, B., Chan, W.T., Swenson, D., Sacchettini, J.C., Jacobs, W.R., Jr., and Russell, D.G. (2000). Persistence of Mycobacterium tuberculosis in macrophages and mice requires the glyoxylate shunt enzyme isocitrate lyase. Nature *406*, 735–738.

Motyl, M., Dorso, K., Barrett, J., and Giacobbe, R. (2006). Basic microbiological techniques used in antibacterial drug discovery. Curr. Protoc. Pharmacol. *13*, 13A.3.

Muñoz-Elías, E.J., and McKinney, J.D. (2005). Mycobacterium tuberculosis isocitrate lyases 1 and 2 are jointly required for in vivo growth and virulence. Nat. Med. *11*, 638–644.

Murshudov, G.N., Skubák, P., Lebedev, A.A., Pannu, N.S., Steiner, R.A., Nicholls, R.A., Winn, M.D., Long, F., and Vagin, A.A. (2011). REFMAC5 for the refinement of macromolecular crystal structures. Acta Crystallogr. D Biol. Crystallogr. *67*, 355–367.

Nuñez, M.F., Pellicer, M.T., Badia, J., Aguilar, J., and Baldoma, L. (2001). Biochemical characterization of the 2-ketoacid reductases encoded by ycdW and yiaE genes in Escherichia coli. Biochem. J. *354*, 707–715.

Obach, R.S., Baxter, J.G., Liston, T.E., Silber, B.M., Jones, B.C., MacIntyre, F., Rance, D.J., and Wastall, P. (1997). The prediction of human pharmacokinetic parameters from preclinical and in vitro metabolism data. J. Pharmacol. Exp. Ther. *283*, 46–58.

Otwinowski, Z., and Minor, W. (1997). Processing of X-ray Diffraction Data Collected in Oscillation Mode. Methods Enzymol. *276*, 307–326.

Pais, G.C.G., Zhang, X., Marchand, C., Neamati, N., Cowansage, K., Svarovskaia, E.S., Pathak, V.K., Tang, Y., Nicklaus, M., Pommier, Y., et al. (2002). Structure activity of 3-aryl-1,3-diketo-containing compounds as HIV-1 integrase inhibitors. J. Med. Chem. *45*, 3184–3194.

Pettersen, E.F., Goddard, T.D., Huang, C.C., Couch, G.S., Greenblatt, D.M., Meng, E.C., and Ferrin, T.E. (2004). UCSF Chimera—a visualization system for exploratory research and analysis. J. Comput. Chem. *25*, 1605–1612.

Philip, V., Harris, J., Adams, R., Nguyen, D., Spiers, J., Baudry, J., Howell, E.E., and Hinde, R.J. (2011). A survey of aspartate-phenylalanine and glutamate-phenylalanine interactions in the protein data bank: searching for anion-π pairs. Biochemistry *50*, 2939–2950.

Quartararo, C.E., and Blanchard, J.S. (2011). Kinetic and chemical mechanism of malate synthase from Mycobacterium tuberculosis. Biochemistry *50*, 6879–6887.

Rullas, J., García, J.I., Beltrán, M., Cardona, P.J., Cáceres, N., García-Bustos, J.F., and Angulo-Barturen, I. (2010). Fast standardized therapeutic-efficacy assay for drug discovery against tuberculosis. Antimicrob. Agents Chemother. *54*, 2262–2264.

Sakuraba, H., Yoneda, K., Takeuchi, K., Tsuge, H., Katunuma, N., and Ohshima, T. (2008). Structure of an archaeal alanine:glyoxylate aminotransferase. Acta Crystallogr. D Biol. Crystallogr. *64*, 696–699.

Sambandamurthy, V.K., Derrick, S.C., Hsu, T., Chen, B., Larsen, M.H., Jalapathy, K.V., Chen, M., Kim, J., Porcelli, S.A., Chan, J., et al. (2006). Mycobacterium tuberculosis DeltaRD1 DeltapanCD: a safe and limited replicating mutant strain that protects immunocompetent and immunocompromised mice against experimental tuberculosis. Vaccine *24*, 6309–6320.

Schnappinger, D., Ehrt, S., Voskuil, M.I., Liu, Y., Mangan, J.A., Monahan, I.M., Dolganov, G., Efron, B., Butcher, P.D., Nathan, C., and Schoolnik, G.K. (2003). Transcriptional Adaptation of Mycobacterium tuberculosis within Macrophages: Insights into the Phagosomal Environment. J. Exp. Med. *198*, 693–704.

Schottel, B.L., Chifotides, H.T., and Dunbar, K.R. (2008). Anion-pi interactions. Chem. Soc. Rev. *37*, 68–83.

Sharma, V., Sharma, S., Hoener zu Bentrup, K., McKinney, J.D., Russell, D.G., Jacobs, W.R., Jr., and Sacchettini, J.C. (2000). Structure of isocitrate lyase, a persistence factor of Mycobacterium tuberculosis. Nat. Struct. Biol. *7*, 663–668.

Smith, C.V., Huang, C.C., Miczak, A., Russell, D.G., Sacchettini, J.C., and Höner zu Bentrup, K. (2003). Biochemical and structural studies of malate synthase from Mycobacterium tuberculosis. J. Biol. Chem. *278*, 1735–1743.

Summa, V., Petrocchi, A., Pace, P., Matassa, V.G., Francesco, R.D., Altamura, S., Tomei, L., Koch, U., and Neuner, P. (2004). Discovery of alpha,gamma-diketo acids as potent selective and reversible inhibitors of hepatitis C virus NS5b RNA-dependent RNA polymerase. J. Med. Chem. *47*, 14–17.

Talaat, A.M., Lyons, R., Howard, S.T., and Johnston, S.A. (2004). The temporal expression profile of Mycobacterium tuberculosis infection in mice. Proc. Natl. Acad. Sci. USA *101*, 4602–4607.

Timm, J., Post, F.A., Bekker, L.-G., Walther, G.B., Wainwright, H.C., Manganelli, R., Chan, W.-T., Tsenova, L., Gold, B., Smith, I., et al. (2003). Differential expression of iron-, carbon-, and oxygen-responsive mycobacterial genes in the lungs of chronically infected mice and tuberculosis patients. Proc. Natl. Acad. Sci. USA *100*, 14321–14326.

Tumey, L.N., Huck, B., Gleason, E., Wang, J., Silver, D., Brunden, K., Boozer, S., Rundlett, S., Sherf, B., Murphy, S., et al. (2004). The identification and optimization of 2,4-diketobutyric acids as flap endonuclease 1 inhibitors. Bioorg. Med. Chem. Lett. *14*, 4915–4918.

Wayne, L.G., and Lin, K.Y. (1982). Glyoxylate metabolism and adaptation of Mycobacterium tuberculosis to survival under anaerobic conditions. Infect. Immun. *37*, 1042–1049.

World Health Organization (2011). Global Tuberculosis Control 2011. Geneva, Switzerland. http://www.who.int/tb/publications/global_report/en/.

Yazdanian, M., Glynn, S.L., Wright, J.L., and Hawi, A. (1998). Correlating partitioning and caco-2 cell permeability of structurally diverse small molecular weight compounds. Pharm. Res. *15*, 1490–1494.

Zeng, L.-F., Jiang, X.-H., Sanchez, T., Zhang, H.-S., Dayam, R., Neamati, N., and Long, Y.-Q. (2008). Novel dimeric aryldiketo containing inhibitors of HIV-1 integrase: effects of the phenyl substituent and the linker orientation. Bioorg. Med. Chem. *16*, 7777–7787.